

# The Nuclear Physics of Neutron Stars\*

J. Piekarewicz<sup>†</sup>

Department of Physics, Florida State University, Tallahassee, FL 32306, USA

(Dated: October 6, 2022)

Neutron stars—compact objects with masses similar to that of our Sun but radii comparable to the size of a city—contain the densest form of matter in the universe that can be probed in terrestrial laboratories as well as in earth- and space-based observatories. The historical detection of gravitational waves from a binary neutron star merger has opened the brand new era of multimessenger astronomy and has propelled neutron stars to the center of a variety of disciplines, such as astrophysics, general relativity, nuclear physics, and particle physics. The main input required to study the structure of neutron stars is the pressure support generated by its constituents against gravitational collapse. These include neutrons, protons, electrons, and perhaps even more exotic constituents. As such, nuclear physics plays a prominent role in elucidating the fascinating structure, dynamics, and composition of neutron stars.

## I. INTRODUCTION

Among the most interesting questions animating nuclear astrophysics today are: *What are the new states of matter at exceedingly high density and temperature?* and *how were the elements from iron to uranium made?* In one clean sweep, the historical detection of gravitational waves from the binary neutron star merger GW170817 by the LIGO-Virgo collaboration [1] has provided critical insights into the nature of dense matter [2–19] and on the synthesis of the heavy elements in the cosmos [20–23].

The term neutron star appears in writing for the first time in the 1933 proceedings of the American Physical Society by Baade and Zwicky who wrote: *With all reserve we advance the view that supernovae represent the transition from ordinary stars into “neutron stars”, which in their final stages consist of extremely closed packed neutrons* [24]. It appears, however, that a couple of years earlier Landau speculated on the existence of dense stars that look like giant atomic nuclei [25]. The first quantitative calculation of the structure of neutron stars was performed by Oppenheimer and Volkoff in 1939 by employing the full power of Einstein’s theory of general relativity [26]. Using what it is now commonly referred to as the Tolman-Volkoff-Oppenheimer (TOV) equations [26, 27], Oppenheimer and Volkoff predicted that a neutron star supported exclusively by quantum mechanical pressure from its constituent neutrons will collapse into a black hole once its mass exceeds seven tenths of a solar mass, or  $M_{\max} = 0.7M_{\odot}$ . Almost 30 years later, Jocelyn Bell discovered “pulsars” which, after a period of great confusion in which they were mistaken as potential beacons from an extraterrestrial civilization, were finally identified as rapidly rotating neutron stars [28].

Since then, the field has evolved by leaps and bounds, and to date, a few thousands neutron stars have been identified [29]. Among the most impactful discoveries since then is the identification of three neutron stars with masses in the

vicinity of two solar masses [30–33], although a recent publication has reported the observation of a neutron star with an even larger mass of about  $M_{\max} = 2.35M_{\odot}$  [34]. These discoveries suggest that the original prediction by Oppenheimer and Volkoff underestimates the current limit on the maximum neutron star mass by at least a factor of three. It is now known that such dramatic discrepancy is associated with the unrealistic assumption that neutrons behave as a non-interacting gas of fermions. That is, Oppenheimer and Volkoff incorrectly assumed that neutrons in a neutron star behave as electrons in a white-dwarf star. Thus, the mere existence of massive neutron stars highlights the vital role of nuclear interactions in explaining the structure, dynamics, and composition of neutron stars. In this manner, the detailed understanding of neutron stars has been transferred to the domain of nuclear physics.

The TOV equations are model independent as the only assumption behind them is the validity of Einstein’s theory of general relativity. However, the solution of the TOV equation requires a detailed description of the relation between the energy density—which provides the source of gravity—and the pressure—which prevents the gravitational collapse of the star. This relation is enshrined in the equation of state (EOS). Unlike a classical ideal gas where the density is low and the temperature is high, the relevant domain for neutron stars involves high densities and low temperatures. That is, in neutron stars the inter-particle separation is small relative to the thermal de Broglie wavelength, thereby highlighting the role of quantum correlations. That the inter-particle separation in the core of neutron stars is small implies that the dynamics is dominated by the short-distance repulsion of the nucleon-nucleon interaction. Such a repulsion provides an additional source of pressure support above and beyond the Fermi (or Pauli) pressure assumed by Oppenheimer and Volkoff. It is this additional support that becomes essential in supporting massive neutron stars against gravitational collapse. Further, the quantum regime of low temperatures and high densities suggests that neutron stars may effectively be treated as zero-temperature systems. Thus the challenge is to infer the absolute ground state of the system over the enormous range of densities and pressures present in a neutron star.

\* This is a draft of an article that has been accepted for publication by Oxford University Press in the Oxford Research Encyclopedia of Physics edited by Brian Foster due for publication in 2022.

<sup>†</sup> jpiekarewicz@fsu.edu

## II. TOMOGRAPHY OF A NEUTRON STAR

The structure of neutron stars is both interesting and complex. Figure 1 encapsulates our current understanding of the structure and composition of neutron stars [35–37]. The outermost surface of the neutron star contains a very thin atmosphere of only a few centimeters thick that is composed of Hydrogen, but may also contain heavier elements such as Helium and Carbon. The electromagnetic radiation emitted from the surface and collected on earth- and space-based telescopes is instrumental in our determination of some critical parameters of the neutron star. For example, under the assumption of blackbody emission from the stellar surface, one can determine the effective surface temperature  $T$  of the star. Moreover, by invoking the Stefan-Boltzmann law,  $L = 4\pi\sigma R^2 T^4$ , one can in principle infer the radius of the star, a quantity that provides critical information on the equation of state. Unfortunately, complications associated with distance measurements that are required to determine the absolute stellar luminosity  $L$ , as well as atmospheric distortions of the black-body spectrum, make the accurate determination of stellar radii a challenging task [38–40].

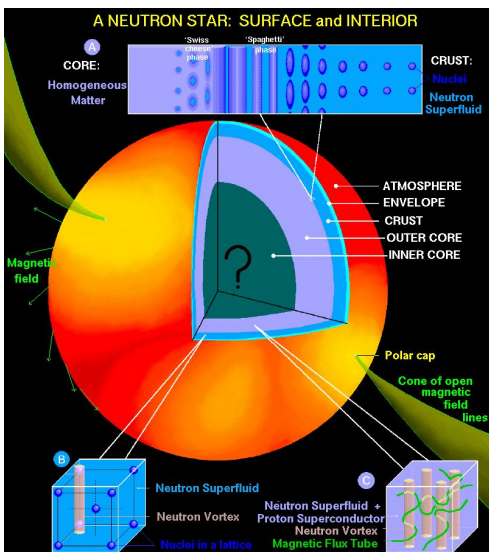


Figure 1. A theoretically-informed rendition of the structure and phases of a neutron star. Courtesy of Dany Page [36].

Fortunately, the situation has improved through a better understanding of systematic uncertainties, important theoretical developments, and the implementation of robust statistical methods [41–48]. More recently, the tidal deformability of neutron stars extracted from GW170817 [1, 5] together with the monitoring of hot spots in neutron stars [49–53], are providing new tools for the accurate determination of stellar radii.

Just below the atmosphere lies a thick envelope that acts as a “blanket” between the hot interior and the relatively cold surface [35]. Matter in this region is not yet fully degenerate so details associated with both the complexity of the atmosphere and large magnetic fields are beyond the nuclear physics purview. However, the layers below, starting with the

solid crust and ending with the high density core, are the main focus of this article. The non-uniform crust represents a region of about 1 km that is composed of a lattice of exotic neutron-rich nuclei immersed in a uniform, neutralizing electron gas and a quantum liquid of superfluid neutrons [54, 55]. Even deeper in the crust, the universal phenomenon of Coulomb frustration favors the formation of a complex set of topological phases dubbed “nuclear pasta” [56, 57]. The non-uniform crust sits above a uniform liquid core that consists of neutrons, protons, electrons, and muons. The core accounts for practically all the mass and for about 90% of the size of a neutron star. Finally, depending on the presently unknown largest density that may be attained in the stellar core, there is also a possibility, marked with a question mark in Fig.1, of a transition into a phase made of exotic particles, such as hyperons, meson condensates, and deconfined quark matter [36].

### A. The Outer Crust

The typical densities encountered in the outer crust of the neutron star span about seven orders of magnitude, from  $10^4 \text{g/cm}^3$  to about  $10^{11} \text{g/cm}^3$  [58]. In this region the average inter-particle separation is significantly larger than the range of the nucleon-nucleon interaction. As such, the system—if arranged in a uniform configuration—would not be able to benefit from the intermediate-range attraction of the nucleon-nucleon interaction. Hence, at these densities it becomes energetically favorable for the system to break the uniform spatial symmetry and to cluster into neutron-rich nuclei segregated into a Coulomb lattice that is immersed in a uniform electron gas. Electrons are an essential component of the neutron star as they enforce the overall charge neutrality of the system. Thus, the constituents of the outer crust are neutrons, protons, and electrons in chemical (or beta) equilibrium.

In the outer crust, and indeed throughout the entire star, the basic question that one needs to answer is how do the relevant constituents organize themselves to minimize the energy over the enormous range of densities encountered in a neutron star. Fortunately, the dynamics of the outer crust is relatively simple, as its dependence on the strong nuclear interaction is fully encapsulated in the masses of a few atomic nuclei. The dynamics of the outer crust is entirely contained in three distinct contributions to the Gibbs free energy of the system: lattice, electronic, and nuclear. The energy associated with the lattice contribution is complicated due to the long-range nature of the Coulomb interaction. It consists of divergent contributions that must be carefully canceled as required by the overall charge neutrality of the system. However, accurate numerical calculations for the electron gas have been available for a long time [59, 60], which have since been adapted to the problem of interest [58, 61, 62]. In turn, the electronic contribution is encoded in the known energy per particle of a relativistic Fermi gas of electrons. All that is left is the nuclear contribution. The nuclear contribution is obtained by identifying the optimal nucleus whose mass per nucleon minimizes the Gibbs free energy per particle at a given pressure. In essence, all one needs to compute the composition of the outer crust is

an accurate nuclear mass table.

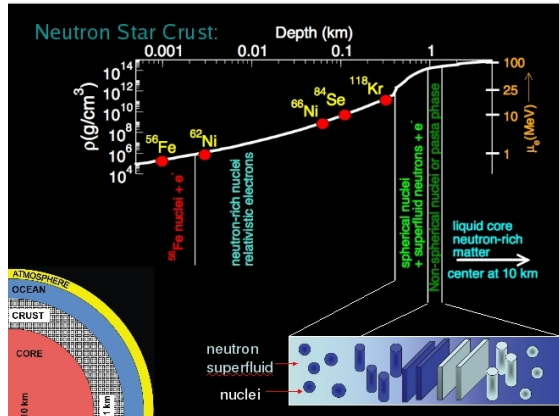


Figure 2. A theoretically-informed rendition of a neutron star with emphasis on the crustal composition. Courtesy of Sanjay Reddy.

At the top layers of the outer crust where the density is lowest, it is energetically favorable for nucleons to cluster into  $^{56}\text{Fe}$  nuclei, which arranged themselves in a face-centered cubic lattice [58]; see Fig. 2. Iron is the optimal nucleus at low density because it has the lowest mass per nucleon in the entire nuclear chart. However, as the density and pressure increase,  $^{56}\text{Fe}$  ceases to be the preferred nucleus. The reason for this behavior is that the electronic contribution to the Gibbs free energy grows rapidly with increasing density/pressure. Thus, it becomes energetically advantageous for the energetic electrons to capture onto protons, making the matter neutron rich. At densities of about  $10^6\text{g/cm}^3$ ,  $^{62}\text{Ni}$  becomes the most favorable nucleus. Note that although  $^{62}\text{Ni}$  has a lower binding energy per nucleon than  $^{56}\text{Fe}$ , it is  $^{56}\text{Fe}$  which has a lower mass per nucleon because its slightly smaller neutron fraction; the entire difference amounts to only 12 keV. For a neutron star in hydrostatic equilibrium, the pressure and density continue to increase as one moves towards the deeper layers of the outer crust. As the density increases, the system evolves into a Coulomb lattice of progressively more exotic, neutron-rich nuclei [61, 62]. Finally, at a neutron-drip density of about  $10^{11}\text{g/cm}^3$ , atomic nuclei are incapable of binding any more neutrons. As suggested in Fig. 2, most of the existing mass models predict that the sequence of progressively more exotic nuclei ends with  $^{118}\text{Kr}$ —a nucleus with 36 protons and 82 neutrons.

Ultimately, the determination of the optimal nucleus is set by a competition between the electron fraction and the nuclear symmetry energy, a concept that appears for the first time in the semi-empirical mass model of Bethe and Weizsäcker [63, 64]. The symmetry energy quantifies the energy cost of turning symmetric nuclear matter, with equal number of protons and neutrons, into pure neutron matter. Low electron fractions diminish the electronic contribution to the Gibbs free energy but at the expense of creating very neutron-rich nuclei. In turn, a large neutron excess is disfavored by the nuclear symmetry energy. Knowledge of the symmetry energy—and especially its density dependence—is one of the most important contributions of nuclear physics to

our understanding of neutron stars.

Given that the last krypton isotope with a well measured mass is  $^{97}\text{Kr}$ , which is still 21 neutrons away from the predicted drip-line nucleus  $^{118}\text{Kr}$ , one must rely on mass models that are often hindered by uncontrolled extrapolations. To mitigate this problem, two important developments have taken place. First, the highly anticipated Facility for Rare Isotope Beams (FRIB) is now up and running. FRIB will surpass current limits of precision and sensitivity that will enable the production of exotic nuclei at or near the drip lines. Second, state-of-the-art mass models [65–71] have been refined by capitalizing on the explosion of machine learning techniques [72–82]. To overcome some of the intrinsic limitations of existing mass models, machine learning approaches have been implemented with the goal of optimizing mass residuals between theory and experiment. Beyond a significant improvement in the predictions of existing models, the Bayesian refinement provides predictions that are accompanied by statistical uncertainties.

Finally, we note that there are three important regions in the nuclear chart that are critical for our understanding of the outer crust: (a) the iron-nickel region, (b) the region around the  $N = 50$  isotones, and (c) the region around the  $N = 82$  isotones. In the case of the iron-nickel region, the masses of all relevant nuclei have been measured with enormous precision. Although not with the same level of precision as in the iron-nickel region, nuclear masses in the neighborhood of the  $N = 50$  isotonic chain have for the most part been measured [83]. For example, in a landmark experiment at ISOLTRAP at CERN, the mass of  $^{82}\text{Zn}$  ( $Z = 30$  and  $N = 52$ ) was measured for the very first time [84]. The addition of this one mass value alone resulted in an interesting modification to the composition of the outer crust [84, 85]. Lastly, very little (if at all!) is known about the masses of the very neutron-rich nuclei in the neighborhood of the  $N = 82$  isotonic chain. It is precisely in this region that machine learning refinements to mass models informed by experiments at FRIB and other rare-isotope facilities will become of utmost importance.

## B. The Inner Crust

The inner stellar crust comprises the region from neutron-drip density up to the density at which uniformity in the system is restored. The exact crust-to-core transition density is unknown, but calculations predict that it lies between a third to a half of nuclear matter saturation density. Based on the nearly uniform interior density of heavy nuclei, nuclear matter saturation density has been determined to be around  $n_0 = 0.15\text{fm}^{-3}$  [86], corresponding to a mass density of  $\rho_0 \approx 10^{14}\text{g/cm}^3$ .

On the top layers of the inner crust, nucleons continue to cluster into a Coulomb crystal of neutron-rich nuclei embedded in a uniform electron gas. However, beyond neutron drip, the crystal is in chemical equilibrium with a superfluid neutron vapor. Most of the evidence in favor of neutron pairing in the crust is obtained from studying its early thermal relaxation period [37]. An interesting consequence of superfluid pairing

is the appearance of pulsar “glitches”. Rotation-powered pulsars tend to spin down slowly and steadily due to the emission of magnetic dipole radiation, making pulsars one of nature’s most accurate clocks. For example, the 33 ms Crab pulsar spins down by about  $13\mu\text{s}$  per year. Despite this remarkable regularity, young pulsars often glitch, a unique phenomenon characterized by a sudden and abrupt spin-up in their rotational frequency. Pulsar timing has revealed that glitches are recurrent, with some of the more active glitchers being the Vela and the Crab pulsars [87]. Although the precise details of the pulsar glitch mechanism are unclear [88, 89], it is believed that the glitch mechanism is intimately related to the formation of superfluid vortices in the inner crust of the rotating neutron star; see Refs.[90–92] and references contained therein. As the pulsar slows down, the initial distribution of vortices that are believed to be pinned to the crystal lattice falls out of equilibrium. This induces a differential rotation between the slower neutron star and the faster superfluid vortices. When the differential lag is too large, then suddenly and abruptly some fraction of the vortices unpin, migrate outwards, and transfer their angular momentum to the solid crust—which is detected as a glitch. After this transient event, the star continues to slow down, stresses between the crust and the superfluid start to build up again until eventually more vortices unpin, transfer angular momentum to the solid crust, and ultimately generate another glitch.

From the perspective of nuclear structure, the most fascinating component of the inner crust is the nuclear pasta phase. In the outer crust and in the top layers of the inner crust, the short-distance scales associated with the strong interaction is well separated from the large distance scales characteristic of the Coulomb repulsion. In this density regime, nucleons bind onto nuclei that are well segregated in a crystal lattice. However, at the bottom layers of the inner crust, these length scales become comparable. Competition between short-range attraction and long-range repulsion leads to a universal phenomenon known as “Coulomb frustration”. Such a competition becomes responsible for the emergence of complex structures of various topologies that are collectively known as nuclear pasta [56, 57].

Most theoretical approaches to the structure and dynamics of the inner crust fall into two broad categories: (a) Mean-field models using accurately calibrated interactions that incorporate quantum effects but miss some important many-body correlations [94–100] and (b) semiclassical Monte Carlo (MC) and Molecular Dynamics (MD) formulations where many-body correlations are treated properly but quantum effects are incorporated in an approximate way [93, 101–108]. Among the virtue of the semi-classical MC/MD approaches is that existing computational resources afford the possibility of simulating an enormous number of particles, thereby minimizing the finite-size effects. For example, Schneider and collaborators have studied the formation of multi domains in the nuclear pasta using a simulation box containing about three million nucleons [106]. Figure 3 displays a snapshot of an early Monte-Carlo simulation for a system of 4,000 nucleons at a density that clearly identifies the formation of non-spherical clusters embedded in a dilute neutron vapor [93, 109]. An-

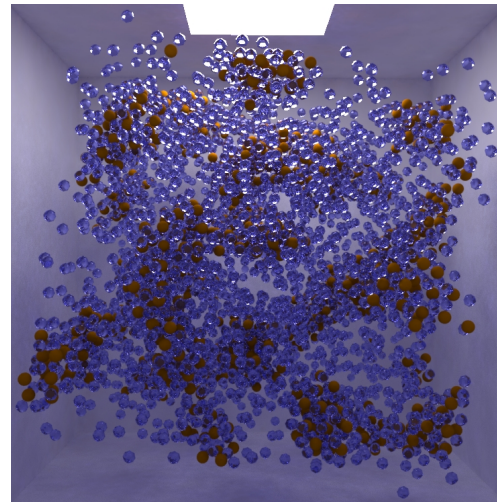


Figure 3. A snapshot of a Monte-Carlo simulation for a system containing 4000 nucleons (3200 neutrons–800 protons) at a baryon density of  $n = n_0/6$  and an effective temperature of  $T = 1$  MeV [93].

other great virtue of the semiclassical simulations is that pasta formation is studied in an unbiased way without assuming any particular set of shapes. Rather, the system evolves dynamically into these complex configurations from an underlying two-body interaction consisting of a short-range nuclear attraction and a long-range Coulomb repulsion. This fact is of great relevance given that one of the main characteristics of Coulomb-frustrated systems, such as the nuclear pasta, is the preponderance of quasi-degenerate ground states. That is, small changes in either the baryon density or the proton fraction can induce dramatic changes in topology, but with only a very modest gain in energy [110]. However, such small changes may have a profound impact on the crustal dynamics and transport properties [93, 109, 111–119].

Finally, whereas the study of nuclear pasta is fascinating in its own right, it may be the key to explain some interesting astrophysical phenomena such as the lack of X-ray-emitting isolated pulsars with long spin periods [120] and the slow cooling rate of MXB 1659-29 [121], a binary system consisting of a neutron star accreting from a low-mass companion star. However, it is unclear how thick the crustal region is that is occupied by the nuclear pasta. This feature—as well as the transition density from the non-uniform crust to the uniform core—depend critically on the poorly known density dependence of the symmetry energy [122]. If the symmetry energy is small at the densities of relevance for pasta formation, then the imbalance between neutrons and protons may be large, thereby reducing the overall long-range repulsion and thus hindering the emergence of the pasta phase; after all, a system made entirely of neutrons does not cluster.

### C. The Outer Core

At densities of about  $10^{14}\text{g}/\text{cm}^3$  the nuclear pasta “melts” and uniformity in the system is restored. Above the crust-

core transition density the original perception of Baade and Zwicky [24] of a neutron star is finally realized: a uniform assembly of extremely closed packed neutrons. At these densities the neutron star consists of neutrons, protons, electrons, and muons in chemical equilibrium. As a result of chemical equilibrium, the proton fraction in the core hovers around 10% with a corresponding fraction of charged leptons required to maintain charge neutrality. Muons are important once the Fermi energy of the electron equals the rest mass of the muon, which happens in the vicinity of nuclear matter saturation density.

Whereas the stellar crust displays fascinating and intriguing dynamics, its structural impact on the star is rather modest. Indeed, with a crustal radius of about 1-2 km, the core accounts for about 90% of the size and most of the mass of the neutron star. Thus, the stellar core provides a unique laboratory for the study of the ground state of uniform, neutron-rich matter over conditions that are unattainable in terrestrial laboratories. By the same reason, the equation of state of neutron-rich matter is poorly constrained by laboratory observables. As articulated later in Sec.III, the most powerful constraints on the EOS between the core-crust transition density and about twice saturation density emerge from a combination of theory and laboratory experiments. The stellar composition in this region is also controlled by the density dependence of the symmetry energy. A stiff symmetry energy, namely, one that increases rapidly with baryon density, disfavors a large neutron-proton asymmetry. This has interesting consequences as a stiff symmetry energy favors large proton fractions that are required for the onset of the direct Urca process [123]. The direct Urca process provides a very efficient mechanism for cooling the star by neutrino emission from direct beta decay and electron capture [35–37, 124]. A recent laboratory experiment that extracted the neutron skin thickness of  $^{208}\text{Pb}$  seems to suggest that the symmetry energy in the vicinity of nuclear saturation density is stiff [125]. One of the many implications of this experiment is the possibility that the onset of direct Urca process happens at relatively low central densities and correspondingly for relatively low mass neutron stars [126]. This is particularly interesting and timely given that x-ray observations suggest that some neutron stars—for example, the neutron star in the low-mass x-ray binary MXB 1659-29—may need a fast neutrino-cooling process [121]. Although there is still much to learn about the dynamics of neutron rich matter in terms of conventional degrees of freedom, perhaps even more exciting is the possible emergence of exotic states of matter, besides the nuclear pasta and Coulomb crystals that populate the stellar crust. At densities above twice saturation density, a region denoted by a question mark in Fig.1, it is plausible that a system of nucleons and charged leptons evolves into others form of matter, such as hyperonic matter, meson condensates, deconfined quark mater, and/or color superconductors. In some cases, the argument in favor for such a transition is based on simple qualitative arguments but in other cases it requires detailed calculations.

#### D. The Inner Core

Qualitatively, the presence of hyperons in the core of neutron star is easy to understand. Hyperons are baryons containing strange quarks and are therefore heavier than the neutrons and protons that populate the outer core. About 20% more massive than a neutron, the  $\Lambda$ -hyperon is a neutral baryon with one each of an up, a down, and a strange quark. At densities exceeding those found in the outer core, it becomes energetically favorable to produce  $\Lambda$ -hyperons rather than to continue to add neutrons to the system. The emergence of hyperons, analogous to the emergence of muons, is thus a simple consequence of the Pauli exclusion principle. Naively, the onset of hyperons should happen around six times nuclear-matter saturation density. However, unlike leptons in high density matter, both nucleons and hyperons are subject to strong interactions in the stellar medium, which are poorly constrained at the short distances of relevance to the inner core. Thus, whereas it is plausible to expect the formation of hyperonic matter in the inner stellar core, the quantitative details of the transition are highly uncertain. Given that transitions to a new state of matter are usually accompanied by a softening of the equation of state, the emergence of hyperons yields maximum neutron-star masses that are inconsistent with observation [30–33]. This problem is commonly referred to in the literature as the “hyperon puzzle” [127–137].

Among the other exotic states of matter that have been proposed to populate the inner stellar core are meson condensates, particularly pion [138–142] and kaon condensates [143–147]. Pions, kaons, and in general mesons are bound states containing one quark and one antiquark. The explanation for the possible emergence of meson condensates in neutron stars is relatively simple. The propagation of a pion or a kaon in the stellar medium can be drastically different from its propagation in free space because of its coupling to “particle-hole” excitations. Unlike most atomic transitions, nuclear excitations often lead to collective modes involving the coherent superposition of many particle-hole pairs. If the effective particle-hole interaction in the medium becomes strong and attractive, the assumed ground state may become unstable against the formation of pion- or kaon-like excitations. Such an instability signals the restructuring of the ground state into a new state of matter in which a fundamental symmetry of the underlying theory is no longer realized in the ground state. In this particular case, the broken symmetry is parity and the new ground state is a pion or a kaon condensate. Given the difficulty in identifying robust astronomical signatures of such exotic states of matter and inspired by early theoretical calculations of pion-like excitations in atomic nuclei [148–150], experiments have searched—unsuccessfully—for precursors of pion condensation in laboratory experiments [151–154]. As in the case of hyperons, the difficulty in identifying the emergence of such exotic states of matter is our poor knowledge of the strong interaction under the extreme conditions present in the stellar core.

Lastly, we address the possibility of matter composed of quarks and gluons populating the inner stellar core. Quarks and gluons are the basic constituents of Quantum Chromo Dy-

namics (QCD) the fundamental theory of the the strong interaction. On purely geometrical grounds one would expect a transition from hadronic matter, in which the quarks and gluons are confined within baryons and mesons, to deconfined quark matter. Given that protons and neutrons have a finite size, one would anticipate a transition to some form of quark matter around a critical density ( $n_c$ ) at which the nucleons start to touch. Assuming a close packing of spheres of radius  $r_0$ , one obtains a surprisingly low critical density of

$$n_c = \left( \frac{3}{4\pi r_0^3} \right) \left( \frac{\pi}{3\sqrt{2}} \right) = \frac{1}{4\sqrt{2}r_0^3} \approx 2n_0, \quad (1)$$

where the expression in the second bracket ( $\sim 0.741$ ) was shown by Gauss in 1831 to be the highest packing fraction, and as an estimate of  $r_0$  we used the charge radius of the proton  $r_0 \approx 0.84$  fm. At  $2n_0$ , QCD is notoriously difficult to solve in the non-perturbative regime, even using some of the most sophisticated theoretical approaches available today. Perhaps a more useful length scale is that at which the average inter-quark separation becomes smaller than the QCD confining scale, so quarks could roam freely throughout the stellar core [29]. However, the naive picture of free-roaming quarks must be revisited because of the attractive interaction between a pair of quarks [155]. As shown by Bardeen, Cooper, and Schrieffer in their seminal work on superconductivity, an arbitrarily weak attractive force may cause a dramatic restructuring of the normal ground state. Under such a paradigm, QCD predicts that at ultra-high densities and low temperatures—where the up, down, and strange quarks are effectively massless—the ground state is a color superconductor with a unique “color-flavor-locking” (CFL) pairing scheme [155–159]. In the CFL phase the exact color symmetry and the approximate flavor symmetry become intertwined [155]. Moreover, in this limit of massless quarks, three-flavor quark matter is automatically neutral without the need to add neutralizing leptons; indeed, “no electrons are required and none are admitted” [158]. Unfortunately, it is now believed that the extreme densities required for the CFL phase

to emerge can not be reached in the stellar cores. So assessing the impact of QCD at the densities of relevance to neutron stars remains an important challenge that is starting to be addressed in the regime in the very high-density regime where QCD is amenable to perturbation theory [160].

### III. TAMING GRAVITY: THE EQUATION OF STATE

The structure of neutron stars emerges from a fierce competition between gravity and the internal pressure support that prevents the collapse of the star. In hydrostatic equilibrium, these two opposing forces are perfectly balanced. The law of universal gravitation formulated by Newton in 1687 posits that two massive particles attract each other with a force that is proportional to the product of their masses and inversely proportional to the square of their separation. From all fundamental forces of nature—gravity, electromagnetism, weak, and strong—only gravity is always attractive. Such a picture finds its natural explanation in Einstein’s theory of general relativity that attributes the attraction to the curvature of space-time that all objects—both massive and massless—experience as they travel through space. Although Newton’s law of universal gravitation is adequate for the description of the motion of planets around the Sun, the gravitational effects around a neutron star are so strong that modifications to Newtonian gravity are required.

#### A. The Tolman-Oppenheimer-Volkoff Equations

The structure of neutron stars is encoded in the Tolman-Volkoff-Oppenheimer (TOV) equations [26, 27], which represent the generalization of Newtonian gravity to the domain of general relativity. For static, spherically symmetric stars in hydrostatic equilibrium the TOV equations may be written as a pair of coupled, first order differential equations:

$$\frac{dP(r)}{dr} = -\frac{G}{c^2} \frac{(\epsilon(r) + P(r)) \left( M(r) + 4\pi r^3 \frac{P(r)}{c^2} \right)}{r^2 \left( 1 - 2GM(r)/c^2 r \right)} \rightarrow -\frac{G\rho(r)M(r)}{r^2}, \quad (2a)$$

$$\frac{dM(r)}{dr} = 4\pi r^2 \frac{\epsilon(r)}{c^2} \rightarrow 4\pi r^2 \rho(r), \quad (2b)$$

where  $G$  is Newton’s gravitational constant and  $c$  is the speed of light in vacuum. The structural information is contained in  $M(r)$ ,  $\epsilon(r)$ ,  $P(r)$ , and  $\rho(r)$ , which represent the enclosed mass, energy density, pressure, and mass density profiles, respectively. The arrows in the above expressions represent the Newtonian limit of the TOV equations. These limits are ob-

tained by assuming that the corrections from general relativity are negligible, as in the case of white-dwarf stars [161–164].

Once two boundary conditions are provided in terms of a central pressure  $P(0) = P_c$  and an enclosed mass at the origin  $M(0) = 0$ , the TOV equations may be solved numerically using a suitable differential-equation solver, such as the Runge-

Kutta algorithm [165]. The solution of the TOV equations over a wide range of central pressures can then be used to generate the entire mass-radius relation, often regarded as the “holy grail” of neutron star structure. Once these equations are solved, the radius  $R$  and mass  $M$  of the neutron star are obtained as  $P(R) = 0$  and  $M = M(R)$ . That is, the radius is determined as the point at which the pressure goes to zero and the total mass as the value of the enclosed mass at such radius. We note in passing that with the exception of a few (mostly academic choices), the TOV equations must be solved numerically. This, however, presents some non-trivial challenges associated with the diversity of scales involved in the problem. Neutrons, with a mass of  $m \approx 2 \times 10^{-27}$  kg, provide most of the pressure support against the gravitational collapse of a neutron star with a typical mass comparable to that of our own Sun  $M_{\odot} \approx 2 \times 10^{30}$  kg. This represents a mismatch in mass scales of 57 orders of magnitude. Thus, in order to avoid computer overflows—and as important, to gain critical insights into the problem—one must properly rescale the TOV equations [164]. It is interesting to point out that there are approximately  $10^{57}$  neutrons in a neutron star, an astronomical number that makes Avogadro’s number of  $\sim 10^{23}$  pale in comparison!

The validity of general relativity and the existence of a source of pressure support is all that is needed to derive the TOV equations. However, to solve the equations one must in addition provide an equation of state to connect the pressure to the energy density at zero temperature. The best known EOS is that of a classical ideal gas. However, unlike the low densities and high temperatures that define a classical ideal gas, neutron stars are highly-degenerate compact objects where quantum effects are critical. In the quantum regime applicable to neutron stars, the average inter-particle separation is considerably smaller than the thermal de Broglie wavelength, so the fermionic (and bosonic if relevant) nature of the constituents plays a critical role. Moreover, whereas treating the constituents as a non-interacting Fermi gas may be adequate in the description of white-dwarf stars, assuming that neutrons/protons in the stellar interior may be described as a non-interacting Fermi gas is woefully inadequate. Indeed, it was precisely such an assumption by Oppenheimer and Volkoff that led them to predict a maximum neutron star mass of only  $M_{\max} = 0.7 M_{\odot}$  [26, 27], a prediction that is known to be in stark disagreement with the observation of  $\gtrsim 2 M_{\odot}$  neutron stars [30–33]. This underscores the critical role that strong interactions play in the description of neutron stars. In what follows, we discuss the various sources of pressure support and how recent theoretical, experimental, and observational advances are providing a new windows into the EOS.

## B. The Equation of State Ladder

Given that neutron stars would inevitably collapse into black holes in the absence of pressure support, a detailed understanding of the equation of state is critical. To do so, it is convenient to frame the discussion in terms of an “EOS ladder” akin to the cosmic distance ladder used in cosmology.

In Fig.4, each rung in the ladder represents a theoretical, experimental, or observational technique that informs the EOS in a suitable density regime. The first rung in the ladder invokes chiral effective field theory, a purely theoretical approach rooted in the symmetries of QCD [166] and which has its strongest impact on the EOS at and below saturation density. The next rung in the ladder includes laboratory experiments that constrain the EOS in the vicinity of saturation density. Beyond twice saturation density but still below the maximum density found in neutron stars, the EOS is informed by both electromagnetic observations and gravitational wave detections. For the highest densities anticipated to exist in the stellar core, the most stringent constraints are obtained from the identification of the most massive neutron stars. Finally, the last rung in the ladder is motivated by a recent claim that perturbative QCD may impose some constraints on the EOS of neutron-star matter [160]. The result is somehow surprising given that QCD is estimated to become perturbative above 40 times nuclear matter saturation density. Still, perturbative QCD may be effective in excluding some equations of state displaying some extreme behavior. In the next few sections we elaborate on the role of each rung in the ladder. First, however, we start by explaining the marginal role that nuclear interactions play in generating the pressure support in the neutron star crust.

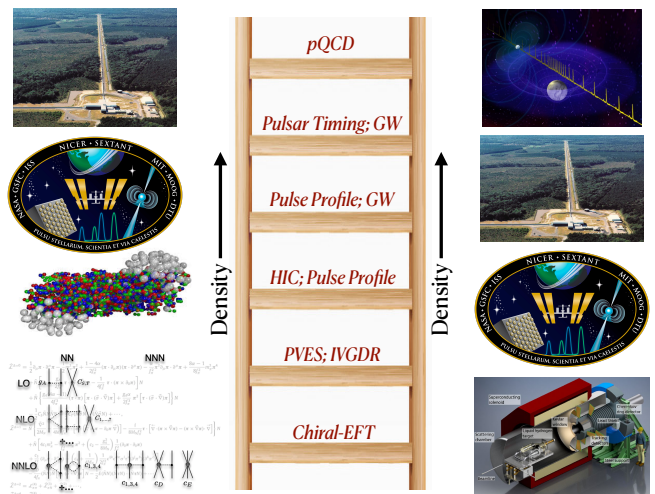


Figure 4. The nuclear equation of state ladder. Akin to the cosmic distance ladder in cosmology, the equation of state ladder represents a succession of theoretical, experimental and observational methods to determine how the pressure changes with increasing density. Given that the range of densities spanned in a neutron star is enormous, no single method can determine the entire EOS. Instead, each rung of the ladder provides information that can be used to determine the EOS at a neighboring rung.

Although the structure of the crust with all its exotic phases is fascinating, the role of nuclear degrees of freedom and their interactions on supporting the crust is marginal, since most of the pressure support is provided by the degenerate electrons. Still, there are some interesting nuclear-structure effects that must be taken into consideration. For example, lack of experimental information on the masses of the neutron-rich

$N = 82$  isotones generates some uncertainty in the composition of the outer crust. Given our limited knowledge of the density dependence of the symmetry energy, this affects the nuclear composition in the bottom layers of the outer crust which, in turn, affects the electron fraction and consequently the pressure support. However, the impact of an uncertain nuclear composition on the EOS is very small. Uncertainties in the inner crust are more severe because the ground state after neutron drip is complex and because no guidance can be obtained from experiment. However, whereas the existence of these exotic phases influence the transport properties in the stellar crust, their impact on the EOS is believed to be rather small [54]. Henceforth, we focus exclusively on the study of the EOS above the crust-core transition density where the system is uniform and nuclear interactions play a predominant role.

### C. Theoretical Constraints

The saturation of symmetric nuclear matter, namely, the existence of a nearly uniform density in the nuclear interior of medium to heavy nuclei is one of the hallmarks of the nuclear dynamics. By the same token, finite nuclei can only provide a very narrow window into the equation of state. Thus, one is forced to resort to theoretical approaches to compute the EOS below saturation density. Using a Quantum Monte Carlo approach, the equation of state of dilute neutron matter has been computed with a simplified interaction that matches smoothly to the known analytic results at very low densities and provides important information at higher densities [167]. The choice of interaction has since been refined by adopting a chiral interaction that is motivated by the underlying symmetries of QCD. One of the great virtues of chiral effective field theory (EFT) is that it provides a systematic and improvable expansion in terms of a suitable small parameter [166, 168, 169]; for a recent review on the application of chiral EFT to the nucleon-nucleon interaction see Ref. [170]. During the last decade, enormous progress has been made in our understanding of the EOS of pure neutron matter by systematically improving the chiral expansion [171–177]. Although the chiral expansion is known to break down above saturation density, high-order chiral EFT calculations of pure neutron matter provide vital constraints on the EOS at and below saturation density [178].

### D. Laboratory Constraints

Laboratory experiments on finite nuclei play an essential role in constraining the EOS of neutron rich matter in the vicinity of saturation density. Although no single technique can be used to determine the EOS over the enormous range of densities spanned in a neutron star, several methods provide insights over a common range of densities, which can then be used to test for consistency and for extending the EOS to the next density rung. In particular, laboratory experiments provide valuable information on the density dependence of the

symmetry energy. Recall that the symmetry energy is related to the energy cost required for converting symmetric nuclear matter into pure neutron matter. In particular, the slope of the symmetry energy at saturation density is closely related to the corresponding pressure of pure neutron matter—a quantity that has already been predicted using chiral EFT [171–177].

The slope of the symmetry energy, a quantity denoted as  $L$ , may also be extracted from laboratory experiments. Although not directly an observable,  $L$  is strongly correlated to the thickness of the neutron skin of heavy nuclei [179–181]. Because of the repulsive Coulomb interaction between protons, heavy nuclei tend to be neutron rich. For example, the nucleus of  $^{208}\text{Pb}$  contains 126 neutrons but only 82 protons. Hence, the root-mean-square radius of the neutron distribution tends to be larger than the radius of the corresponding proton distribution. The difference between the neutron and proton radii is defined as the neutron skin.

But what controls the thickness of the neutron skin? [182]. Although the quantitative value of the neutron skin requires detailed calculations, a qualitative explanation of its size and its strong connection to the slope of the symmetry energy are largely model independent. Surface tension favors the formation of a spherical liquid drop containing all 208 nucleons. However, the symmetry energy increases monotonically in the density region of relevance to atomic nuclei. So the symmetry energy favors moving some of the excess neutrons to the surface where the symmetry energy is lower than in the interior. This, however, increases the surface tension. Ultimately then, the thickness of the neutron skin emerges from a competition between the surface tension and the difference between the value of the symmetry energy in the interior relative to its value at the surface. Such a difference is encoded in the slope of the symmetry energy  $L$ . If this difference is large, namely, there is a significant energy gain by moving some excess neutrons to the surface, then the neutron skin will be thick. Conversely, if the energy cost is low, then the excess neutrons will remain in the core, leading to a thin neutron skin. This suggests a powerful correlation: the larger the value of  $L$  the thicker the neutron skin [183]. Such a robust correlation has been verified using a large set of models that have been calibrated to reproduce well-known properties of finite nuclei [181].

Motivated by the possible impact of a terrestrial experiment in constraining the EOS, a proposal was submitted to the Thomas Jefferson National Accelerator Facility more than 20 years ago. The proposed goal of the experiment was to measure the neutron skin thickness of  $^{208}\text{Pb}$  using parity violating electron scattering; denoted by PVES in Fig.4. By measuring the neutron skin thickness of  $^{208}\text{Pb}$ , one would be able to provide valuable information on  $L$ . Unlike experiments involving strongly-interacting probes, such as pions and protons, PVES is clean because it relies exclusively on electroweak probes. Indeed, the parity-violating asymmetry emerges from the interference of Feynman diagrams involving only the exchange of photons and  $Z^0$  bosons. Moreover, unlike the photon, which is largely insensitive to the neutron distribution, the neutral weak vector boson  $Z^0$  couples strongly to the neutrons, making it an ideal probe to map the neutron density.



The first Lead Radius Experiment (“PREX”) established the existence of a neutron-rich skin in  $^{208}\text{Pb}$  [184, 185], suggesting that the pressure of pure neutron matter is “stiff”, namely, that the pressure increases rapidly with increasing density in the vicinity of saturation density. Unfortunately, the impact of the experiment was hindered by unanticipated large error bars. A second effort aimed at improving the precision of the original experiment was successfully completed and reported a neutron skin thickness that confirmed—with much better precision—that the neutron skin of  $^{208}\text{Pb}$  is thick [125] and, in turn, that the symmetry energy is stiff [126]. Relying on the strong correlation between the neutron skin thickness of  $^{208}\text{Pb}$  and the slope of the symmetry energy [181], one was able to infer a value for  $L$  that systematically overestimates existing limits based on both theoretical approaches and experimental measurements involving strongly-interacting probes. Hence, PREX provides the strongest evidence to date in favor of a stiff EOS around saturation density. Moreover, because neutron-star radii are mostly sensitive to the pressure around twice saturation density [186], PREX constrains both, the thickness of the neutron skin and, although to a lesser extent, the radius of a neutron star [187]. This is a remarkable connection involving objects that differ in size by more than 18 orders of magnitude [188]. Other laboratory experiments, such as those that excite the isovector giant dipole resonance or heavy-ion collisions (IVGDR and HIC in Fig.4) are also sensitive to the density dependence of the symmetry energy. A discussion of the advantages and disadvantages of these and many other experimental techniques may be found in Refs. [189–191].

### E. Observational Constraints I

The first rung in the ladder relies on chiral EFT to determine the EOS at low densities. Piggybacking on this rung, laboratory experiments extend our knowledge of the EOS perhaps as far as twice saturation density. In turn, measurements of stellar radii by the Neutron Star Interior Composition Explorer (NICER) inform the EOS at even higher densities. NICER, launched in June 2017 aboard SpaceX’s Falcon 9 rocket and deployed to the International Space Station, is part of NASA’s first program dedicated to the study of the exotic structure and composition of neutron stars. NICER relies on the powerful technique of Pulse Profile Modeling to monitor electromagnetic emission from the hot spots located on the surface of the neutron star [46, 192]. Magnetic fields in pulsars are so strong and complex that charged particles that are ripped away from the star often crash back into the stellar surface creating hot spots, regions within the star that glow brighter than the rest of the star. As the neutron star spins, the hot spots come in and out of view, producing periodic variations in the brightness, or a distinct pulse profile, that are recorded by NICER’s powerful instruments. Because of gravitational light-bending—one of the most dramatic consequences of the general theory of relativity—hot spots emissions are detected by NICER, even when the emission is coming from the “back” of the star. The more compact the star, the more dramatic the effect. In this

manner, NICER provides critical information on the EOS by constraining the stellar compactness:

$$\frac{v^2}{c^2} = \frac{2GM}{c^2 R} = \frac{R_s}{R}, \quad (3)$$

where  $v$ ,  $M$ ,  $R$ , and  $R_s$  are the escape velocity, mass, radius, and Schwarzschild radius of the star, respectively. The Schwarzschild radius represents the radius at which the neutron star would become a black hole, or equivalently, when the escape velocity from the star would equal the speed of light. For example, a one-solar mass object like our Sun would become a black hole when its radius reaches about 3 km.

Before the deployment of NICER, no single neutron star had both their mass and radius simultaneously determined. This changed in 2019 with the determination of the mass and radius of the millisecond pulsar PSR J0030+0451. Two different groups, one based in Europe [49] and the other one in the United States [50], have provided independent—and fully consistent—estimates. Both groups found that a neutron star with a mass of about 1.4 solar masses has a radius of approximately 13 km [49, 50]. The second target of the NICER mission was the millisecond pulsar PSR J0740+6620 that was selected because, unlike PSR J0030+0451, its mass was previously determined using pulsar timing [32, 33]; see Section III G. For this massive pulsar with a mass of more than twice the mass of the Sun, the extracted neutron star radius was about 12.4 km [51, 52]. In tandem, these two pioneering observations suggest that the equation of state in the relevant density domain is relatively stiff. Moreover, these two measurements appear to validate an earlier conjecture that suggests that neutron stars have approximately the same radius over a wide mass range [41].

### F. Gravitational-Wave Constraints

The historical detection of gravitational waves emitted from the binary neutron star merger GW170817 has opened a brand new window into the Universe [1]. Gravitational waves offer a treasure trove of new information that complements electromagnetic observations of myriad of astrophysical phenomena. In particular, GW170817 started to provide answers to two fundamental questions in nuclear science: (i) What are the new states of matter at exceedingly high density and temperature? and (ii) how were the elements from iron to uranium made?

Just a few hours after the gravitational-wave detection, ground- and space-based telescopes identified the associated electromagnetic transient, or “kilonova”, that is believed to have been powered by the radioactive decay of the heavy elements synthesized in the rapid neutron-capture process [20–23].

Concerning the equation of state, GW170817 provides a few critical observables, such as the chirp mass, the mass ratio, and the tidal deformability. The tidal deformability describes the tendency of a neutron star to develop a mass quadrupole in response to the tidal field generated by its companion star [193, 194]. In the linear regime of small tidal dis-

turbances, the constant of proportionality connecting the tidal forces to the mass quadrupole is the dimensionless tidal deformability  $\Lambda$  defined as

$$\Lambda = \frac{2}{3}k_2 \left( \frac{c^2 R}{GM} \right)^5 = \frac{64}{3}k_2 \left( \frac{R}{R_s} \right)^5, \quad (4)$$

where  $k_2$  is the second Love number [195, 196]. Although  $k_2$  is sensitive to the underlying EOS, most of the sensitivity is contained in the compactness parameter [3, 197–203]. Indeed, for a given mass, the tidal deformability scales approximately as the fifth power of the stellar radius, a quantity that has been notoriously difficult to constrain before NICER and LIGO-Virgo [38–41, 48]. In particular, an estimate by the LIGO-Virgo collaboration of the tidal deformability of a  $1.4 M_{\text{sun}}$  neutron star yields the relatively small value of  $\Lambda_{1.4} \lesssim 580$ , suggesting that neutron stars are compact objects that are difficult to tidally deform [5]. Such a small value for the tidal deformability translates into a stellar radius of approximately  $R_{1.4} = 11.4 \text{ km}$  [204]. Although consistent within error bars, such a low central value for  $R_{1.4}$  differs significantly from the  $R_{1.4} = 13 \text{ km}$  radius extracted from the first NICER observation. To our knowledge, GW170817 provides one of the very few indications that the EOS is soft.

Besides the tidal deformability, other observables of relevance to the EOS are encoded in the gravitational waveform. To leading order in the post-Newtonian expansion—an expansion in terms of the ratio of the orbital velocity to the speed of light—the gravitational-wave signal is determined by the “chirp” mass, which involves a linear combination of the individual stellar masses [205]. To determine the individual masses one must invoke higher orders in the post-Newtonian expansion [206]. Although the individual masses of GW170817 could not be determined very precisely, the extracted upper limit on the most massive of the two stars [1] did not challenge the present maximum-mass limit of about  $2.1 M_{\odot}$ . This situation could have changed dramatically with the detection of gravitational waves from the coalescence of a binary system GW190814 with the most extreme mass ratio ever observed: a 23 solar mass black hole and a 2.6 solar mass compact object [207]. The LIGO-Virgo collaboration suggested that GW190814 is unlikely to have originated from a neutron star-black hole coalescence, yet left open the possibility that improved knowledge of the equation of state or future observations could alter this assessment.

Within a theoretical framework uniquely suited to investigate both the properties of finite nuclei and neutron stars, it was concluded that the low deformability demanded by GW170817 combined with heavy-ion data, make it highly unlikely that neutron stars can have masses as large as  $2.6 M_{\odot}$  [208]. The absence of very massive neutron stars is also consistent with the analysis by Margalit and Metzger who argue against their formation based on the lack of evidence of a large amount of rotational energy in the ejecta during the spin-down phase of GW170817 [209]. Interestingly, the suggested upper limit of  $M_{\text{max}} \lesssim 2.17 M_{\odot}$  [209] is in full agreement with the recent observation by Cromartie and collaborators of the most massive neutron star to date [32, 33]. Yet the mystery remains unsolved, as the existence of black holes

with a mass as small as  $2.6 M_{\odot}$  is also problematic. It has even been suggested that GW190814 may have been a second-generation merger from a hierarchical triple system: a binary neutron star coalescence leading to the  $2.6 M_{\odot}$  compact object that ultimately merges with the  $23 M_{\odot}$  black hole [210]. Finally, the detection of massive neutron stars from the binary coalescence complements pulsar timing techniques that provide the most precise information to date on massive neutron stars and forms the last observational rung in the EOS ladder.

## G. Observational Constraints II

According to Newton’s law of universal gravitation, all that can be determined from the motion of two orbiting objects is their combined mass. This fact is encapsulated in Kepler’s third law of planetary motion:

$$P^2 = \frac{4\pi^2}{G(M_1 + M_2)} a^3, \quad (5)$$

where  $P$  is the orbital period,  $a$  is the length of the semi-major axis of the ellipse, and  $M_1$  and  $M_2$  are the individual masses of the two orbiting bodies. To determine the individual masses one must go beyond Newtonian mechanics and invoke general relativity. The most successful observational technique used to determine the individual masses is pulsar timing. The success of pulsar timing in extracting orbital parameters stems from the remarkable precision of pulsars in keeping time. These celestial timekeepers often rival the precision of the most sophisticated atomic clocks. Millisecond pulsars form a distinct group of recycled neutron stars that rotate extremely fast. It is believed that the rapid rotation involves a spin-up during mass accretion from a companion star. Further, this class of pulsars generate weak magnetic fields of “only” about 100 million Gauss, leading to very small energy losses due to magnetic dipole radiation. The fast rotation and the weak magnetic fields make pulsars extremely stable clocks with minuscule spin-down rates of about 1 second every trillion years! Long-time observations of millisecond pulsars that account for each rotation provide a precise determination of the orbital parameters.

Shapiro delay [211], regarded as the fourth test of general relativity, is a powerful technique that has been used in combination with pulsar timing to infer the mass of the companion star, thereby breaking the mass degeneracy encountered in Newtonian gravity. The main concept behind the Shapiro delay is that even massless particles, such as photons, bend as they pass near massive objects because of the curvature of space-time. This causes a time delay in the arrival of the electromagnetic radiation emitted by the neutron star as it passes near the companion star on its way to the observer. In accounting for every rotation of the neutron star over long periods of time, pulsar timing together with Shapiro delay provide a highly precise value for the mass of the companion star. Once the mass degeneracy has been broken, Kepler’s law may then be used to extract the mass of the neutron star. This powerful technique was used back in 2010 to determine

both the mass of the pulsar J1614-2230 and of its companion white-dwarf star [30]. In particular, the mass of the neutron star was found to be close to two solar masses, providing the first serious challenge to models that predict soft equations of state due to the emergence of exotic states of matter. Recently, Shapiro delay was used to measure the mass of the millisecond pulsar J0740+6620, that with a mass of about  $M = 2.1 M_{\odot}$  is the most massive—well measured—neutron star to date [32, 33]; although see [34]. Note that the millisecond pulsar J0740+6620 is one of the two neutron stars that was targeted by the NICER mission and for which a radius measurement now exists [51, 52].

## H. Conclusions

So what can we conclude from the wealth of information that we have gathered during the last five years? Figure 5 encapsulates some of the information obtained from laboratory experiments (PREX-2), electromagnetic observations (NICER), and gravitational-wave detections (LIGO-Virgo). Predictions are displayed from a set of models that reproduce properties of finite nuclei and generate an equation of state stiff enough to support neutron stars with masses of at least  $2M_{\odot}$ . At the  $1\sigma$  level, PREX-2 disfavors models that predict a neutron skin thickness in  $^{208}\text{Pb}$  of less than  $R_{\text{skin}} = 0.21 \text{ fm}$  [125], suggesting that the EOS in the vicinity of saturation density is stiff [126]. In turn, the two magenta horizontal lines indicate the radius of a  $M = 1.4M_{\odot}$  neutron star as reported by the two independent analyses of the NICER data [49, 50]. Although differing by 18 orders of magnitude in size and probing different regions of the EOS, both PREX-2 and NICER favor a relatively stiff equation of state. However, some tension emerges as we incorporate the tidal deformability of a  $M = 1.4M_{\odot}$  neutron star extracted from GW170817. Combining two analyses [1, 5], the recommended upper limit for the tidal deformability was reported to be 580 at the 90% confidence level. As it stands, all models displayed in the figure will be inconsistent with such an upper limit. Such a softening of the EOS at intermediate densities—bracketed by a stiff EOS at both low densities and high densities as suggested by PREX-2 and massive neutron stars, respectively, may be indicative of a phase transition in the stellar interior [3]. While enormously exciting, one must wait for the next generation of experimental and observational facilities to validate such a scenario.

Finally, Fig.6 displays the holy grail of neutron-star structure, namely, the mass-radius (MR) relation informed by the many pioneering developments in the field. Mass constraints obtained from electromagnetic observations of the three most massive neutron stars to date are shown with the horizontal bars [30–33]. In turn, the two horizontal arrows in the figure indicate constraints on stellar radii obtained exclusively from GW170817, suggesting that the equation of state in the relevant density region is soft [2, 3]. Such a scenario excludes several models that predict larger stellar radii. By measuring relatively large radii for PSR J0030 and PSR J0740, NICER has relaxed some of the tight constraint imposed by GW170817.

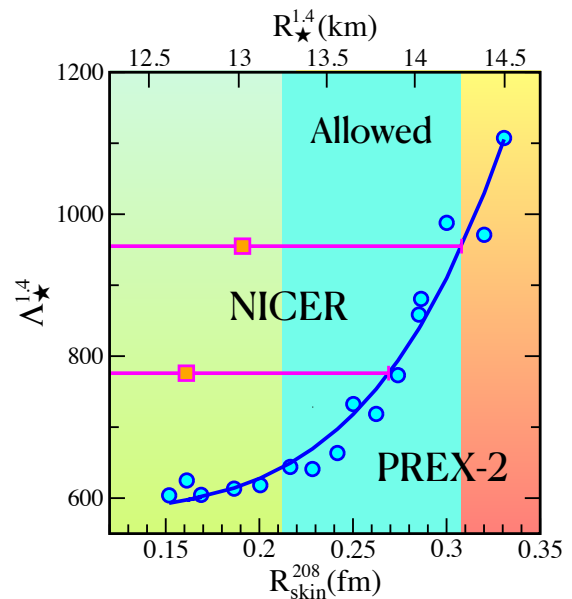


Figure 5. Experimental and Observational constraints on theoretical models of the equation of state, with its predictions denoted by the blue dots. Results are shown for the neutron skin thickness of  $^{208}\text{Pb}$ , together with the tidal deformability and radius of a  $M = 1.4M_{\odot}$  neutron star. The combined PREX-II result together with NICER constraints on the stellar radius is depicted by the small (blue) window of models allowed [126].

NICER results are denoted in the figure by the horizontal error bars located at about  $M = 1.4M_{\odot}$  and  $M = 2M_{\odot}$ . The excluded causality region was adopted from Ref.[186]. Relative to the status of the field five years ago, the progress in tightening the MR relation—and consequently the EOS—is simply remarkable.

In summary, due a confluence of pioneering developments in a variety of interconnected disciplines, we have entered the golden era of neutron stars [212, 213]. Remarkable advances are anticipated across all these disciplines during the next few years. Among these, the operation of brand new terrestrial facilities that will measure the properties of atomic nuclei at the limits of existence, new telescopes operating across the entire electromagnetic spectrum that will determine with unprecedented precision the mass-radius relation, and future gravitational-wave observatories that will make countless detections of gravitational waves from compact binary coalescence. Such remarkable developments, combined with advances in our theoretical understanding of dense, neutron-rich matter, will ultimately lead to a detailed understanding of the structure, dynamics, and composition of neutron stars, arguably, among the most fascinating objects in the universe.

## ACKNOWLEDGMENTS

I am grateful to all my colleagues—especially my graduate students—that contributed to this work and to the community that has made the study of neutron stars one of the most exciting endeavors in all of nuclear science. This material is based

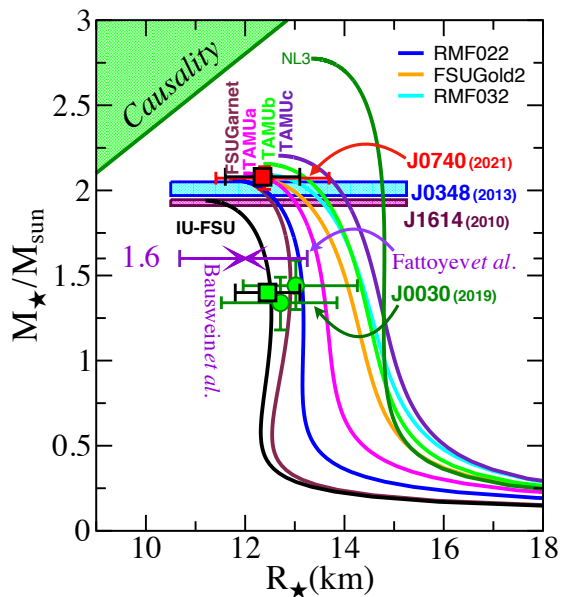


Figure 6. The “Holy-Grail” of nuclear-star structure: The Mass-Radius relation as predicted by a set of theoretical models. The historical detection of gravitational waves, the precise measurement of heavy neutron stars, the simultaneous determinations of the mass and radius of two neutron stars, and the extraction of the neutron-skin thickness of a heavy nucleus are shaping our advances in determining the MR relation and ultimately the equation of state of neutron rich matter.

upon work supported by the U.S. Department of Energy Office of Science, Office of Nuclear Physics under Award Number DE-FG02-92ER40750.

- 
- [1] B. P. Abbott *et al.* (Virgo, LIGO Scientific), *Phys. Rev. Lett.* **119**, 161101 (2017).
- [2] A. Bauswein, O. Just, H.-T. Janka, and N. Stergioulas, *Astrophys. J.* **850**, L34 (2017).
- [3] F. J. Fattoyev, J. Piekarewicz, and C. J. Horowitz, *Phys. Rev. Lett.* **120**, 172702 (2018).
- [4] E. Annala, T. Gorda, A. Kurkela, and A. Vuorinen, *Phys. Rev. Lett.* **120**, 172703 (2018).
- [5] B. P. Abbott *et al.* (Virgo, LIGO Scientific), *Phys. Rev. Lett.* **121**, 161101 (2018).
- [6] E. R. Most, L. R. Weih, L. Rezzolla, and J. Schaffner-Bielich, *Phys. Rev. Lett.* **120**, 261103 (2018).
- [7] I. Tews, J. Margueron, and S. Reddy, *Phys. Rev.* **C98**, 045804 (2018).
- [8] T. Malik, N. Alam, M. Fortin, C. Providencia, B. K. Agrawal, T. K. Jha, B. Kumar, and S. K. Patra, *Phys. Rev.* **C98**, 035804 (2018).
- [9] D. Radice, A. Perego, F. Zappa, and S. Bernuzzi, *Astrophys. J. Lett.* **852**, L29 (2018).
- [10] D. Radice and L. Dai, *Eur. Phys. J. A* **55**, 50 (2019).
- [11] I. Tews, J. Margueron, and S. Reddy, *Eur. Phys. J. A* **55**, 97 (2019).
- [12] C. D. Capano, I. Tews, S. M. Brown, B. Margalit, S. De, S. Kumar, D. A. Brown, B. Krishnan, and S. Reddy, *Nature Astronomy* **4**, 625 (2019).
- [13] M. Tsang, W. Lynch, P. Danielewicz, and C. Tsang, *Phys. Lett. B* **795**, 533 (2019).
- [14] C. Y. Tsang, M. B. Tsang, P. Danielewicz, W. G. Lynch, and F. J. Fattoyev, *Phys. Rev. C* **102**, 045808 (2020).
- [15] C. Drischler, R. Furnstahl, J. Melendez, and D. Phillips, *Phys. Rev. Lett.* **125**, 202702 (2020).
- [16] P. Landry, R. Essick, and K. Chatziioannou, *Phys. Rev. D* **101**, 123007 (2020).
- [17] W.-J. Xie and B.-A. Li, *Phys. Rev. C* **103**, 035802 (2021).
- [18] R. Essick, I. Tews, P. Landry, and A. Schwenk, *Phys. Rev. Lett.* **127**, 192701 (2021).
- [19] K. Chatziioannou, *Phys. Rev. D* **105**, 084021 (2022).
- [20] M. R. Drout *et al.*, *Science* **358**, 1570 (2017).
- [21] P. S. Cowperthwaite *et al.*, *Astrophys. J.* **848**, L17 (2017).
- [22] R. Chornock *et al.*, *Astrophys. J.* **848**, L19 (2017).
- [23] M. Nicholl *et al.*, *Astrophys. J.* **848**, L18 (2017).
- [24] W. Baade and F. Zwicky, *Phys. Rev.* **45**, 138 (1934).
- [25] D. G. Yakovlev, P. Haensel, G. Baym, and C. J. Pethick, *Phys. Usp.* **56**, 289 (2013), arXiv:1210.0682 [physics.hist-ph].
- [26] J. R. Oppenheimer and G. M. Volkoff, *Phys. Rev.* **55**, 374 (1939).
- [27] R. C. Tolman, *Phys. Rev.* **55**, 364 (1939).
- [28] A. Hewish, S. Bell, J. Pilkington, P. Scott, and R. Collins, *Nature* **217**, 709 (1968).
- [29] J. M. Lattimer and M. Prakash, *Science* **304**, 536 (2004).
- [30] P. Demorest, T. Pennucci, S. Ransom, M. Roberts, and J. Hessels, *Nature* **467**, 1081 (2010).
- [31] J. Antoniadis, P. C. Freire, N. Wex, T. M. Tauris, R. S. Lynch, *et al.*, *Science* **340**, 6131 (2013).
- [32] H. T. Cromartie *et al.*, *Nat. Astron.* **4**, 72 (2019).
- [33] E. Fonseca *et al.*, (2021), arXiv:2104.00880 [astro-ph.HE].
- [34] R. W. Romani, D. Kandel, A. V. Filippenko, T. G. Brink, and W. Zheng, *Astrophys. J. Lett.* **934**, L18 (2022).

- [35] D. Page, J. M. Lattimer, M. Prakash, and A. W. Steiner, *Astrophys. J. Suppl.* **155**, 623 (2004).
- [36] D. Page and S. Reddy, *Ann. Rev. Nucl. Part. Sci.* **56**, 327 (2006).
- [37] D. Page, J. M. Lattimer, M. Prakash, and A. W. Steiner, *Astrophys. J.* **707**, 1131 (2009).
- [38] F. Ozel, G. Baym, and T. Guver, *Phys. Rev.* **D82**, 101301 (2010).
- [39] A. W. Steiner, J. M. Lattimer, and E. F. Brown, *Astrophys. J.* **722**, 33 (2010).
- [40] V. Suleimanov, J. Poutanen, M. Revnitsev, and K. Werner, *Astrophys. J.* **742**, 122 (2011).
- [41] S. Guillot, M. Servillat, N. A. Webb, and R. E. Rutledge, *Astrophys. J.* **772**, 7 (2013).
- [42] J. M. Lattimer and A. W. Steiner, *Astrophys. J.* **784**, 123 (2014).
- [43] C. O. Heinke, H. N. Cohn, P. M. Lugger, N. A. Webb, W. Ho, *et al.*, *Mon. Not. Roy. Astron. Soc.* **444**, 443 (2014).
- [44] S. Guillot and R. E. Rutledge, *Astrophys. J.* **796**, L3 (2014).
- [45] F. Ozel, D. Psaltis, T. Guver, G. Baym, C. Heinke, and S. Guillot, *Astrophys. J.* **820**, 28 (2016).
- [46] A. L. Watts *et al.*, *Rev. Mod. Phys.* **88**, 021001 (2016).
- [47] A. W. Steiner, C. O. Heinke, S. Bogdanov, C. Li, W. C. G. Ho, A. Bahramian, and S. Han, *Mon. Not. Roy. Astron. Soc.* **476**, 421 (2018).
- [48] J. Nattila, M. C. Miller, A. W. Steiner, J. J. E. Kajava, V. F. Suleimanov, and J. Poutanen, *Astron. Astrophys.* **608**, A31 (2017).
- [49] T. E. Riley *et al.*, *Astrophys. J. Lett.* **887**, L21 (2019).
- [50] M. C. Miller *et al.*, *Astrophys. J. Lett.* **887**, L24 (2019).
- [51] M. C. Miller *et al.*, *Astrophys. J. Lett.* **918**, L28 (2021).
- [52] T. E. Riley *et al.*, *Astrophys. J. Lett.* **918**, L27 (2021).
- [53] G. Raaijmakers, S. K. Greif, K. Hebel, T. Hinderer, S. Nisanke, A. Schwenk, T. E. Riley, A. L. Watts, J. M. Lattimer, and W. C. G. Ho, (2021), arXiv:2105.06981 [astro-ph.HE].
- [54] N. Chamel and P. Haensel, *Living Rev. Rel.* **11**, 10 (2008).
- [55] C. Bertulani and J. Piekarewicz, "Neutron star crust." (Nova Science Publishers, Hauppauge New York, 2012).
- [56] D. G. Ravenhall, C. J. Pethick, and J. R. Wilson, *Phys. Rev. Lett.* **50**, 2066 (1983).
- [57] M. Hashimoto, H. Seki, and M. Yamada, *Prog. Theor. Phys.* **71**, 320 (1984).
- [58] G. Baym, C. Pethick, and P. Sutherland, *Astrophys. J.* **170**, 299 (1971).
- [59] R. A. Coldwell-Horsfall and A. A. Maradudin, *Journal of Mathematical Physics* **1**, 395 (1960).
- [60] C. A. Sholl, *Proceedings of the Physical Society* **92**, 434 (1967).
- [61] S. B. Ruester, M. Hempel, and J. Schaffner-Bielich, *Phys. Rev.* **C73**, 035804 (2006).
- [62] X. Roca-Maza and J. Piekarewicz, *Phys. Rev.* **C78**, 025807 (2008).
- [63] H. A. Bethe and R. F. Bacher, *Rev. Mod. Phys.* **8**, 82 (1936).
- [64] C. F. von Weizsäcker, *Z. Physik* **96**, 431 (1935).
- [65] J. Duflo, *Nucl. Phys.* **A576**, 29 (1994).
- [66] J. Duflo and A. Zuker, *Phys. Rev.* **C52**, R23 (1995).
- [67] P. Möller, J. R. Nix, and K. L. Kratz, *Atom. Data Nucl. Data Tabl.* **66**, 131 (1996).
- [68] P. Möller, W. D. Myers, H. Sagawa, and S. Yoshida, *Phys. Rev. Lett.* **108**, 052501 (2012).
- [69] S. Goriely, N. Chamel, and J. M. Pearson, *Phys. Rev. Lett.* **102**, 152503 (2009).
- [70] S. Goriely, N. Chamel, and J. M. Pearson, *Phys. Rev.* **C88**, 061302 (2013).
- [71] M. Kortelainen, T. Lesinski, J. More, W. Nazarewicz, J. Sarich, *et al.*, *Phys. Rev.* **C82**, 024313 (2010).
- [72] K. Gernoth, J. Clark, J. Prater, and H. Bohr, *Phys. Lett. B* **300**, 1 (1993).
- [73] J. W. Clark and H. Li, *Int. J. Mod. Phys.* **B20**, 5015 (2006).
- [74] S. Athanassopoulos, E. Mavrommatis, K. A. Gernoth, and J. W. Clark, *Nucl. Phys.* **A743**, 222 (2004).
- [75] R. Utama, J. Piekarewicz, and H. B. Prosper, *Phys. Rev.* **C93**, 014311 (2016).
- [76] R. Utama and J. Piekarewicz, *Phys. Rev.* **C96**, 044308 (2017).
- [77] R. Utama and J. Piekarewicz, *Phys. Rev.* **C97**, 014306 (2018).
- [78] L. Neufcourt, Y. Cao, W. Nazarewicz, and F. Viens, *Phys. Rev.* **C98**, 034318 (2018).
- [79] L. Neufcourt, Y. Cao, W. Nazarewicz, E. Olsen, and F. Viens, *Phys. Rev. Lett.* **122**, 062502 (2019).
- [80] L. Neufcourt, Y. Cao, S. A. Giuliani, W. Nazarewicz, E. Olsen, and O. B. Tarasov, *Phys. Rev. C* **101**, 044307 (2020).
- [81] Z. M. Niu and H. Z. Liang, *Phys. Lett. B* **778**, 48 (2018).
- [82] A. E. Lovell, A. T. Mohan, T. M. Sprouse, and M. R. Mumpower, *Phys. Rev. C* **106**, 014305 (2022).
- [83] S. Giraud *et al.*, *Phys. Lett. B* **833**, 137309 (2022).
- [84] R. Wolf *et al.*, *Phys. Rev. Lett.* **110**, 041101 (2013).
- [85] J. Pearson, S. Goriely, and N. Chamel, *Phys. Rev.* **C83**, 065810 (2011).
- [86] C. J. Horowitz, J. Piekarewicz, and B. Reed, *Phys. Rev. C* **102**, 044321 (2020).
- [87] "Jodrell Bank Centre for Astrophysics (glitch catalogue) <http://www.jb.man.ac.uk/pulsar/glitches.html>,".
- [88] N. Andersson, K. Glampedakis, W. Ho, and C. Espinoza, *Phys. Rev. Lett.* **109**, 241103 (2012).
- [89] N. Chamel, *Phys. Rev. Lett.* **110**, 011101 (2013).
- [90] P. Anderson and N. Itoh, *Nature* **256**, 25 (1975).
- [91] M. Alpar, S. Langer, and J. Sauls, *Astrophys. J.* **282**, 533 (1984).
- [92] D. Pines and M. Alpar, *Nature* **316**, 27 (1985).
- [93] C. J. Horowitz, M. A. Perez-Garcia, and J. Piekarewicz, *Phys. Rev.* **C69**, 045804 (2004).
- [94] T. Maruyama, T. Tatsumi, D. N. Voskresensky, T. Tanigawa, and S. Chiba, *Phys. Rev.* **C72**, 015802 (2005).
- [95] S. Avancini, D. Menezes, M. Alloy, J. Marinelli, M. Moraes, *et al.*, *Phys. Rev.* **C78**, 015802 (2008).
- [96] W. Newton and J. Stone, *Phys. Rev.* **C79**, 055801 (2009).
- [97] S. S. Avancini, C. C. Barros, Jr, L. Brito, S. Chiacchiera, D. P. Menezes, and C. Providencia, *Phys. Rev.* **C85**, 035806 (2012).
- [98] B. Schuetrumpf and W. Nazarewicz, *Phys. Rev.* **C92**, 045806 (2015).
- [99] F. Fattoyev, C. Horowitz, and B. Schuetrumpf, *Phys. Rev. C* **95**, 055804 (2017).
- [100] W. G. Newton, M. A. Kaltenborn, S. Cantu, S. Wang, A. Stinson, and J. Rikowska Stone, *Phys. Rev. C* **105**, 025806 (2022).
- [101] G. Watanabe, K. Sato, K. Yasuoka, and T. Ebisuzaki, *Phys. Rev.* **C68**, 035806 (2003).
- [102] G. Watanabe, T. Maruyama, K. Sato, K. Yasuoka, and T. Ebisuzaki, *Phys. Rev. Lett.* **94**, 031101 (2005).
- [103] G. Watanabe, H. Sonoda, T. Maruyama, K. Sato, K. Yasuoka, *et al.*, *Phys. Rev. Lett.* **103**, 121101 (2009).
- [104] J. Piekarewicz and G. Toledo Sanchez, *Phys. Rev.* **C85**, 015807 (2012).
- [105] M. E. Caplan, A. S. Schneider, C. J. Horowitz, and D. K. Berry, *Phys. Rev.* **C91**, 065802 (2015).
- [106] A. da Silva Schneider, M. E. Caplan, D. K. Berry, and C. J. Horowitz, *Phys. Rev. C* **98**, 055801 (2018).
- [107] J. A. Lopez, C. O. Dorso, and G. A. Frank, *Front. Phys. (Bei-*

- jing) **16**, 24301 (2021).
- [108] R. Shafieepour, H. R. Moshfegh, and J. Piekarewicz, *Phys. Rev. C* **105**, 055809 (2022).
- [109] C. J. Horowitz, M. A. Perez-Garcia, J. Carriere, D. K. Berry, and J. Piekarewicz, *Phys. Rev. C* **70**, 065806 (2004).
- [110] R. A. Kycia, S. Kubis, and W. Wójcik, *Phys. Rev. C* **96**, 025803 (2017).
- [111] C. J. Horowitz, M. A. Perez-Garcia, D. K. Berry, and J. Piekarewicz, *Phys. Rev. C* **72**, 035801 (2005).
- [112] C. J. Horowitz and D. K. Berry, *Phys. Rev. C* **78**, 035806 (2008).
- [113] C. J. Horowitz and K. Kadau, *Phys. Rev. Lett.* **102**, 191102 (2009).
- [114] P. Grygorov, P. Gogelein, and H. Muther, *J.Phys.G* **G37**, 075203 (2010).
- [115] N. Chamel, *Phys. Rev. C* **85**, 035801 (2012).
- [116] C. J. Horowitz, D. K. Berry, C. M. Briggs, M. E. Caplan, A. Cumming, and A. S. Schneider, *Phys. Rev. Lett.* **114**, 031102 (2015).
- [117] M. E. Caplan and C. J. Horowitz, *Rev. Mod. Phys.* **89**, 041002 (2017).
- [118] R. Nandi and S. Schramm, *Astrophys. J.* **852**, 135 (2018).
- [119] Z. Lin, M. E. Caplan, C. J. Horowitz, and C. Lunardini, *Phys. Rev. C* **102**, 045801 (2020).
- [120] J. A. Pons, D. Viganó, and N. Rea, *Nature Physics*, **9**, 431-434 (2013).
- [121] E. F. Brown, A. Cumming, F. J. Fattoyev, C. Horowitz, D. Page, and S. Reddy, *Phys. Rev. Lett.* **120**, 182701 (2018).
- [122] C. J. Horowitz and J. Piekarewicz, *Phys. Rev. Lett.* **86**, 5647 (2001).
- [123] C. J. Horowitz and J. Piekarewicz, *Phys. Rev. C* **66**, 055803 (2002).
- [124] J. M. Lattimer, M. Prakash, C. J. Pethick, and P. Haensel, *Phys. Rev. Lett.* **66**, 2701 (1991).
- [125] D. Adhikari *et al.* (PREX), *Phys. Rev. Lett.* **126**, 172502 (2021).
- [126] B. T. Reed, F. J. Fattoyev, C. J. Horowitz, and J. Piekarewicz, *Phys. Rev. Lett.* **126**, 172503 (2021).
- [127] I. Vidana, A. Polls, A. Ramos, L. Engvik, and M. Hjorth-Jensen, *Phys. Rev. C* **62**, 035801 (2000).
- [128] F. Sammarruca, *Phys. Rev. C* **79**, 034301 (2009).
- [129] S. Weissenborn, D. Chatterjee, and J. Schaffner-Bielich, *Phys. Rev. C* **85**, 065802 (2012), [Erratum: *Phys.Rev.C* **90**, 019904 (2014)].
- [130] E. Massot, J. Margueron, and G. Chanfray, *EPL* **97**, 39002 (2012).
- [131] D. Lonardoni, A. Lovato, S. Gandolfi, and F. Pederiva, *Phys. Rev. Lett.* **114**, 092301 (2015).
- [132] M. Oertel, F. Gulminelli, C. Providência, and A. R. Raduta, *Eur. Phys. J. A* **52**, 50 (2016).
- [133] M. Oertel, M. Hempel, T. Klähn, and S. Typel, *Rev. Mod. Phys.* **89**, 015007 (2017).
- [134] L. Tolos, M. Centelles, and A. Ramos, *Astrophys. J.* **834**, 3 (2017).
- [135] M. Fortin, S. S. Avancini, C. Providência, and I. Vidaña, *Phys. Rev. C* **95**, 065803 (2017).
- [136] J. Negreiros, L. Tolos, M. Centelles, A. Ramos, and V. Dexheimer, *Astrophys. J.* **863**, 104 (2018).
- [137] D. Logoteta, *Universe* **7**, 408 (2021).
- [138] R. F. Sawyer, *Phys. Rev. Lett.* **29**, 382 (1972).
- [139] A. B. Migdal, *Phys. Lett. B* **45**, 448 (1973).
- [140] G. Baym and E. Flowers, *Nucl. Phys. A* **222**, 29 (1974).
- [141] W. Weise and G. E. Brown, *Phys. Lett. B* **58**, 300 (1975).
- [142] A. B. Migdal, *Rev. Mod. Phys.* **50**, 107 (1978).
- [143] D. B. Kaplan and A. E. Nelson, *Phys. Lett. B* **175**, 57 (1986).
- [144] G. E. Brown, V. Thorsson, K. Kubodera, and M. Rho, *Phys. Lett. B* **291**, 355 (1992).
- [145] V. Thorsson, M. Prakash, and J. M. Lattimer, *Nucl. Phys. A* **572**, 693 (1994), [Erratum: *Nucl.Phys.A* **574**, 851 (1994)].
- [146] N. K. Glendenning and J. Schaffner-Bielich, *Phys. Rev. Lett.* **81**, 4564 (1998).
- [147] A. Ramos, J. Schaffner-Bielich, and J. Wambach, *Lect. Notes Phys.* **578**, 175 (2001).
- [148] H. Toki and W. Weise, *Phys. Lett. B* **92**, 265 (1980).
- [149] W. M. Alberico, M. Ericson, and A. Molinari, *Phys. Lett. B* **92**, 153 (1980).
- [150] W. M. Alberico, M. Ericson, and A. Molinari, *Nucl. Phys. A* **379**, 429 (1982).
- [151] J. B. McClelland *et al.*, *Phys. Rev. Lett.* **69**, 582 (1992).
- [152] X. Y. Chen *et al.*, *Phys. Rev. C* **47**, 2159 (1993).
- [153] L. Wang *et al.*, *Phys. Rev. C* **50**, 2438 (1994).
- [154] V. R. Pandharipande, J. Carlson, S. C. Pieper, R. B. Wiringa, and R. Schiavilla, *Phys. Rev. C* **49**, 789 (1994).
- [155] F. Wilczek, *Physics Today* **53**, 22 (2000).
- [156] M. G. Alford, K. Rajagopal, and F. Wilczek, *Nucl. Phys.* **B537** (1999), 10.1016/S0550-3213(98)00668-3.
- [157] M. G. Alford, K. Rajagopal, and F. Wilczek, *Phys. Lett. B* **422**, 247 (1998).
- [158] K. Rajagopal and F. Wilczek, *Phys. Rev. Lett.* **86**, 3492 (2001).
- [159] M. G. Alford, A. Schmitt, K. Rajagopal, and T. Schafer, *Rev. Mod. Phys.* **80**, 1455 (2008).
- [160] E. Annala, T. Gorda, A. Kurkela, J. Nättilä, and A. Vuorinen, *Nature Phys.* **16**, 907 (2020).
- [161] A. C. Phillips, “The physics of stars,” (John Wiley & Sons, Chichester, 1998) 2nd ed.
- [162] F. Weber, “Pulsars as astrophysical laboratories for nuclear and particle physics,” (Institute of Physics Publishing, Bristol, UK, 1999).
- [163] N. K. Glendenning, “Compact stars,” (Springer-Verlag New York, 2000).
- [164] J. Piekarewicz, “Neutron star matter equation of state,” in *Handbook of Supernovae*, edited by A. W. Alsabti and P. Murdin (Springer International Publishing, Cham, 2016) pp. 1–20.
- [165] W. H. Press, B. P. Flannery, S. A. Teukolsky, and W. T. Vetterling, “Numerical recipes: The art of scientific computing,” (Cambridge University Press, 1989).
- [166] S. Weinberg, *Phys. Lett. B* **251**, 288 (1990).
- [167] A. Gezerlis and J. Carlson, *Phys. Rev. C* **81**, 025803 (2010).
- [168] U. van Kolck, *Phys. Rev. C* **49**, 2932 (1994).
- [169] C. Ordonez, L. Ray, and U. van Kolck, *Phys. Rev. C* **53**, 2086 (1996).
- [170] D. Rodriguez Entem, R. Machleidt, and Y. Nosyk, *Front. in Phys.* **8**, 57 (2020).
- [171] K. Hebeler and A. Schwenk, *Phys. Rev. C* **82**, 014314 (2010).
- [172] I. Tews, T. Kruger, K. Hebeler, and A. Schwenk, *Phys. Rev. Lett.* **110**, 032504 (2013).
- [173] T. Kruger, I. Tews, K. Hebeler, and A. Schwenk, *Phys. Rev. C* **88**, 025802 (2013).
- [174] D. Lonardoni, I. Tews, S. Gandolfi, and J. Carlson, *Phys. Rev. Res.* **2**, 022033 (2020).
- [175] C. Drischler, J. W. Holt, and C. Wellenhofer, *Ann. Rev. Nucl. Part. Sci.* **71**, 403 (2021).
- [176] F. Sammarruca and R. Millerson, *Phys. Rev. C* **104**, 034308 (2021).
- [177] F. Sammarruca and R. Millerson, *Universe* **8**, 133 (2022).
- [178] M. G. Alford, L. Brodie, A. Haber, and I. Tews, (2022), arXiv:2205.10283 [nucl-th].
- [179] B. A. Brown, *Phys. Rev. Lett.* **85**, 5296 (2000).

- [180] R. J. Furnstahl, Nucl. Phys. **A706**, 85 (2002).
- [181] X. Roca-Maza, M. Centelles, X. Viñas, and M. Warda, Phys. Rev. Lett. **106**, 252501 (2011).
- [182] J. Piekarewicz and F. J. Fattoyev, Physics Today **72**, 30 (2019).
- [183] C. J. Horowitz and J. Piekarewicz, Phys. Rev. **C64**, 062802 (2001).
- [184] S. Abrahamyan, Z. Ahmed, H. Albatineh, K. Aniol, D. S. Armstrong, *et al.*, Phys. Rev. Lett. **108**, 112502 (2012).
- [185] C. J. Horowitz, Z. Ahmed, C. M. Jen, A. Rakhman, P. A. Souder, *et al.*, Phys. Rev. **C85**, 032501 (2012).
- [186] J. M. Lattimer and M. Prakash, Phys. Rept. **442**, 109 (2007).
- [187] J. Carriere, C. J. Horowitz, and J. Piekarewicz, Astrophys. J. **593**, 463 (2003).
- [188] J. Yang and J. Piekarewicz, Ann. Rev. Nucl. Part. Sci. **70**, 21 (2020).
- [189] M. Tsang, J. Stone, F. Camera, P. Danielewicz, S. Gandolfi, *et al.*, Phys.Rev. **C86**, 015803 (2012).
- [190] C. J. Horowitz, E. F. Brown, Y. Kim, W. G. Lynch, R. Michaels, *et al.*, J. Phys. **G41**, 093001 (2014).
- [191] M. Thiel, C. Sfienti, J. Piekarewicz, C. J. Horowitz, and M. Vanderhaeghen, J. Phys. **G46**, 093003 (2019).
- [192] D. Psaltis, F. Özel, and D. Chakrabarty, Astrophys. J. **787**, 136 (2014).
- [193] T. Damour, M. Soffel, and C.-m. Xu, Phys. Rev. **D45**, 1017 (1992).
- [194] E. E. Flanagan and T. Hinderer, Phys. Rev. **D77**, 021502 (2008).
- [195] T. Binnington and E. Poisson, Phys. Rev. **D80**, 084018 (2009).
- [196] T. Damour, A. Nagar, and L. Villain, Phys. Rev. **D85**, 123007 (2012).
- [197] T. Hinderer, Astrophys. J. **677**, 1216 (2008).
- [198] T. Hinderer, B. D. Lackey, R. N. Lang, and J. S. Read, Phys. Rev. **D81**, 123016 (2010).
- [199] T. Damour and A. Nagar, Phys. Rev. **D80**, 084035 (2009).
- [200] S. Postnikov, M. Prakash, and J. M. Lattimer, Phys. Rev. **D82**, 024016 (2010).
- [201] F. J. Fattoyev, J. Carvajal, W. G. Newton, and B.-A. Li, Phys. Rev. **C87**, 015806 (2013).
- [202] A. W. Steiner, S. Gandolfi, F. J. Fattoyev, and W. G. Newton, Phys. Rev. **C91**, 015804 (2015).
- [203] J. Piekarewicz and F. J. Fattoyev, Phys. Rev. C **99**, 045802 (2019).
- [204] R. Essick, I. Tews, P. Landry, S. Reddy, and D. E. Holz, Phys. Rev. C **102**, 055803 (2020).
- [205] B. P. Abbott *et al.* (LIGO Scientific, Virgo), Annalen Phys. **529**, 1600209 (2017).
- [206] C. Cutler and E. E. Flanagan, Phys. Rev. **D49**, 2658 (1994).
- [207] R. Abbott *et al.* (LIGO Scientific, Virgo), Astrophys. J. **896**, L44 (2020).
- [208] F. J. Fattoyev, C. J. Horowitz, J. Piekarewicz, and B. Reed, Phys. Rev. C **102**, 065805 (2020).
- [209] B. Margalit and B. D. Metzger, Astrophys. J. **850**, L19 (2017).
- [210] W. Lu, P. Beniamini, and C. Bonnerot, Mon. Not. Roy. Astron. Soc. **500**, 1817 (2020).
- [211] I. I. Shapiro, Phys. Rev. Lett. **13**, 789 (1964).
- [212] G. Baym, *Proceedings of the 8th International Conference on Quarks and Nuclear Physics (QNP2018)*, 10.7566/JPS-SCP.26.011001.
- [213] G. Baym, T. Hatsuda, T. Kojo, P. D. Powell, Y. Song, and T. Takatsuka, Rept. Prog. Phys. **81**, 056902 (2018).